Disentangling Entanglement Spectra of Fractional Quantum Hall States on Torus Geometries

Andreas M. Läuchli,[1] Emil J. Bergholtz,[1] Juha Suorsa,[2] and Masudul Haque[1]

[1]*Max-Planck-Institut für Physik komplexer Systeme, Nöthnitzer Straße 38, D-01187 Dresden, Germany*
[2]*Department of Physics, University of Oslo, Post Office Box 1048, Blindern, 0316 Oslo, Norway*

We analyze the entanglement spectrum of Laughlin states on the torus and show that it is arranged in towers, each of which is generated by modes of two spatially separated chiral edges. This structure is present for all torus circumferences, which allows for a microscopic identification of the prominent features of the spectrum by perturbing around the thin-torus limit.

Introduction.—The description of condensed matter phases using entanglement measures, borrowed from the field of quantum information theory, has led to an explosive growth of interdisciplinary work [1]. Despite all this interest, there are few cases where entanglement concepts provide physical information that is not obtainable through more conventional quantities, such as correlation functions. One example involves topologically ordered states, for which bipartite entanglement measures have been shown to be useful probes [2–4]. Fractional quantum Hall (FQH) states of two-dimensional electrons in a magnetic field stand out as experimentally realized topologically ordered phases, and have recently received renewed intense attention partly due to quantum computation proposals based on their topological properties [5]. An intriguing feature of FQH states is that their edges have gapless modes, described by chiral Luttinger liquids [6,7]. In this work, we study the interplay of two edges, through the study of *entanglement spectra.*

We focus on bipartite entanglement between two parts (*A* and *B*) of the system. The entanglement spectrum (ES), $\{\xi_i\}$, is defined in terms of the Schmidt decomposition

$$|\psi\rangle = \sum_i e^{-\xi_i/2} |\psi_i^A\rangle \otimes |\psi_i^B\rangle.$$

Here, $|\psi\rangle$ is the ground state, and the states $|\psi_i^A\rangle$ ($|\psi_i^B\rangle$) form an orthonormal basis for the subsystem *A* (*B*).

Very recently, ES studies have been used [4,8] to probe edge modes of FQH states. The entanglement between two partitions of an edgeless wave function may seem at first sight unrelated to edge physics. However, studies of ES in noninteracting systems [9,10] have found that the entanglement spectrum is also the spectrum of an effective "entanglement Hamiltonian" confined to the *A* region of space, which is not identical but similar to the original physical Hamiltonian. If this similarity holds for interacting systems, the low-lying ES would then show an edge structure, even though the total system has no edge. References [4,8] analyzed the ES of FQH states on the sphere with hemispheric partitioning. The Virasoro multiplet structure of the conformal field theory (CFT) describing the edge appear in the low-lying part of the ES.

In this Letter, we present and analyze the entanglement spectrum of $\nu = 1/3$ Laughlin states on the torus. This choice of geometry gives us access to new physics and new analysis tools, compared to the spherical case. The natural partitions of the torus are cylinderlike segments with two disjoint edges. The ES thus contains the physics of a combination of two separate conformal edges. We show that this leads to "towers" in the ES spectrum, when plotted against appropriate quantum numbers. Even in cases where the two edges have different spectra, the two spectra combine to form towers. The two-edge picture provides significant predictive power, as the assignment of only a few edge mode energies enables us to construct the remaining ES.

The torus geometry also allows us to adiabatically connect to the "thin-torus" limit, which is exactly solvable [11,12] and has as ground states the Tao-Thouless crystalline states [13]. Many features of the ES can be understood starting from these simple states, such as the positions of towers and relationships between their energetics. The CFT tower structure persists even very close to the thin-torus limit, which by itself is an uncorrelated product state.

Geometry and partitioning.—We study an *N*-electron system on a torus with periods L_1, L_2 in the *x* and *y* directions, satisfying $L_1 L_2 = 2\pi N_s$ (in units of the magnetic length). Here, $N_s = N/\nu$ is the number of magnetic flux quanta. In the Landau gauge, $\mathbf{A} = By\hat{\mathbf{x}}$, a basis of single
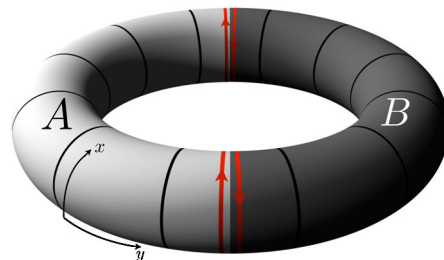

FIG. 1 (color online). Torus setup for block entanglement computations. The lowest Landau level is spanned by orbitals which in Landau gauge are centered along the circles shown. The arrows indicate the chiralities of the virtual "edges" created by the block partitioning.

particle states in the lowest Landau level can be taken as
$$\psi_j = \pi^{-1/4} L_1^{-1/2} \sum_m e^{i[(2\pi/L_1)j + mL_2]x} e^{-[y+(2\pi/L_1)j + mL_2]^2/2}$$
with $j = 0, 1, \ldots, N_s - 1$. The states ψ_j are centered along the lines $y = -2\pi j/L_1$ (Fig. 1). Thus, the y position is given by the x momentum j.

Any translation-invariant two-body interaction Hamiltonian, acting in the lowest Landau level, can be written as

$$H = \sum_n \sum_{k>|m|} V_{km} c_{n+m}^\dagger c_{n+k}^\dagger c_{n+m+k} c_n, \qquad (1)$$

where $c_m^\dagger$ creates an electron in the state ψ_m and V_{km} is the amplitude for two particles to hop symmetrically from separation $k + m$ to $k - m$. Hence, the problem of interacting electrons in a Landau level maps onto a one-dimensional, center-of-mass conserving lattice model with lattice constant $2\pi/L_1$. The Laughlin states at $\nu = 1/3$ are, for all L_1, the unique zero energy grounds states of the pseudopotential interaction $V_{km}^{(1)} = (k^2 - m^2)e^{-2\pi^2(k^2+m^2)/L_1^2}$ [11]. For generic interactions, e.g., the Coulomb interaction, the matrix elements have a more complicated L_1 dependence. Our ES data are extracted from ground states of (1), obtained using the Lanczos algorithm for numerical diagonalization.

We bipartition the system into blocks A and B which consist of l_A consecutive orbitals and the remaining $N_s - l_A$ orbitals, respectively (Fig. 1). Since the orbitals are localized, this is a reasonable approximation to spatial partitioning, as on the sphere [4,8,14,15]. In this Letter, we focus on half-partitioning, $l_A = N_s/2$, and organize the ES in sectors labeled by the particle number, N_A, and the total x momentum, $K_A \bmod N_s$, in the A block.

The $\nu = 1/3$ Laughlin state is threefold degenerate on the torus. The degenerate states are related by translation, and correspond to three different thin-torus configurations:

010|010010|010
100|100100|100 .
001|001001|001

These states are, for generic (including Coulomb and pseudopotential) interactions, adiabatically connected to the bulk ground states without gap closing for any L_1 [11,12]. If the A partition is taken to be the six middle orbitals, the block boundaries are different for the three cases: 0-0 cuts in the first case ("symmetric cut"), a 1-0 and a 0-1 cut in the other two ("asymmetric cuts").

Tower structure and CFT identification.—Numerical ES are shown in Fig. 2 for a 12-particle Laughlin state ($N_s = 36$). A prominent feature is that the ES consists of "towers." Most of the towers are symmetric, while some are skewed. We interpret each tower as a combination of chiral modes of two edges (two block boundaries). An *ad hoc* assignment of a small number of (Virasoro) energies provides the necessary input for constructing each tower.

The number of independent modes of a chiral $U(1)$ CFT at momentum k is given by the partition function $p(k) = 1, 1, 2, 3, 5, 7, 11, \ldots$ for $k = 0, 1, 2, \ldots$. When two *linearly* dispersing chiral modes combine, one expects an ideal tower of states like the one shown in Fig. 2 (inset). The diagonal sequences along the left and right sides are from the individual edges, and so have degeneracies $p(|\Delta K_A|)$ at momentum shifted by ΔK_A from the tower center. A right-moving mode at energy E_1 and momentum k_1 and a left-moving mode at E_2 and momentum $-k_2$ will combine to give a mode at energy $E_1 + E_2$ and momentum $k_1 - k_2$. The rest of the tower is obtained from the states of the two edges through such combinations. Here, energies are measured with respect to the vacuum state at $\Delta K_A = 0$.

The observed towers in the numerical ES can be explained by postulating the individual edge spectra to have
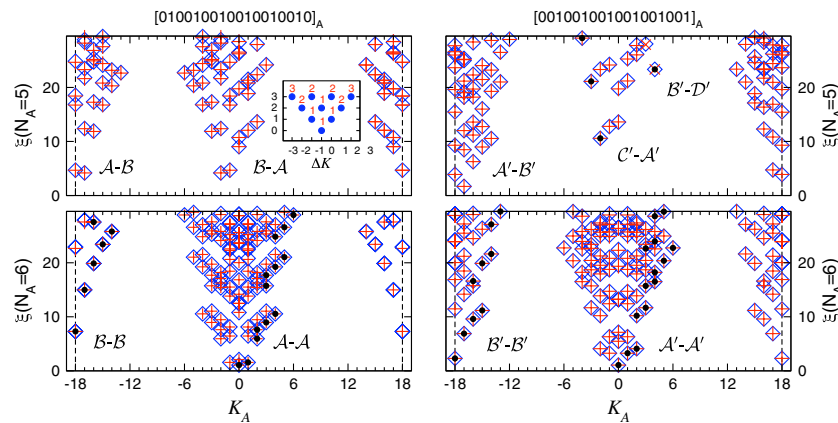

FIG. 2 (color online). Entanglement spectrum for $N_s = 36$ and $L_1 = 10$. Left panels show the symmetric cut and right panels show one of the asymmetric cuts. The origin of K_A is chosen to match the Tao-Thouless state. The blue squares represent numerically obtained data. The assigned edge modes are labeled by black dots while the combinations of those edges are marked by red crosses. The script letters are microscopic identifiers for the two edges combining to form each tower (see text). The striking correspondence of the red crosses with numerical data shows that our algorithm based on the two-edge picture allows the reconstruction of the entire entanglement spectrum using only the positions of the black dots. The inset shows a CFT tower formed by two ideal chiral edges, the states labeled with their degeneracies.

split degeneracies while preserving the Virasoro counting. Two such modified edge spectra can be combined to construct towers which are less degenerate than the ideal case of Fig. 2 (inset). Following this scheme, for the numerical ES towers (Fig. 2), we assigned appropriate levels on the right and left of each tower to single-edge spectra. Several edges in the $N_A \neq N/2$ sectors are identical to edges in the $N_A = N/2$ sector, and thus do not need to be independently assigned. As a result, the energies of a remarkably small number of single-edge states (black dots in Fig. 2) are sufficient to generate the entire ES. This is a key result of the present work.

The assigned single-edge levels have robust relative positions for varying torus thickness [Fig. 3(a)]. The relative positions correspond well to the single-edge levels extracted from ES on a sphere [15], as shown in Fig. 3(a).

Microscopic "thin-torus" analysis.—The adiabatic connection to the thin-torus ($L_1 \to 0$) limit enables us to understand features of the ES by perturbing the solvable limit. In particular, the location and energetics of towers can be understood from such microscopic considerations.

We first consider the symmetric cut and explain the towers in the left panels of Fig. 2. The very lowest ES level is found at $K_A = 0$ in the $N_A = 6$ sector (left bottom panel), and corresponds to the thin-torus configuration

$$010010010 \mid \underbrace{01001001001001010}_{A} \mid 010010010.$$

At $L_1 = 0$, this amounts to the only entanglement level, and for all finite L_1, its dressed counterpart remains at the very bottom of the main tower. The remaining states of this tower are all generated from this by V_{km} processes [Eq. (1)] which conserve N_A. In particular, the leading levels are generated by processes with small k and m. For example, a V_{21} process at the right edge, $0010|0100 \to 0001|1000$, gives the root configuration for the lowest entanglement level at $\Delta K_A = 1$, and at the left edge, this gives the lowest $\Delta K_A = -1$ level. The energetics of the tower is deter-

mined by the microscopic structure of its edges. We refer to this particular environment, 10010|01001, and the corresponding edge energetics as $\mathcal{A}$.

Some processes do not conserve N_A. For the symmetric cut, the leading such process is V_{42} which can change N_A by ± 1: $0010|01001 \to 0000|1110$. We call such an edge environment $\mathcal{B}$, which combines with $\mathcal{A}$ type edges to form the observed $\mathcal{A}$-$\mathcal{B}$ and $\mathcal{B}$-$\mathcal{A}$ towers in the $N_A = 5$ sector. Mirror images of these exist in the $N_A = 7$ sector. By creating two $\mathcal{B}$ edges, one finds that there are two ways of obtaining the $\mathcal{B}$-$\mathcal{B}$ tower in the $N_A = 6$ sector, each with momentum shift $\pm l_A$ ($= \pm N_s/2$) compared to the main tower. The extra twofold degeneracy is seen in our data. The large momentum transfer is because a particle leaves block A at one cut, and one enters A at the opposite cut. We also predict and observe a nondegenerate $\mathcal{B}$-$\mathcal{B}$ tower in the $N_A = 4$ sector (not shown).

We now turn to the asymmetric cut (right panels of Fig. 2). Again, the thin-torus ground state corresponds to the lowest level in the main tower (at $K_A = 0$ in the $N_A = 6$ sector). The two edges, 0100|1001 and 1001|0010, are both denoted $\mathcal{A}'$ as they are each others' mirror images and hence have equivalent energetics. In this case, already the leading hopping term, V_{21}, changes N_A leading to the $\mathcal{B}'$ edge, $0100|1001 \to 0011|0001$. Another edge $\mathcal{C}'$ is generated by the V_{54} process, $1001001|001001 \to 0001111|000001$. A feature of the ES for the asymmetric cut is that the skewed towers within a given N_A sector do not in general have mirror image in that sector. Instead, the mirror images show up in the $(N - N_A)$ sector. Note that the energy of the lowest $\Delta K_A = 0$ state for each tower (tower vacuum energy) is also fixed by the two edges.

Pursuing the microscopic analysis, one can find many nontrivial relations between the energetics in different towers, cuts, and sectors; we have only outlined the basics. It is also possible to derive more quantitative features of the ES as a function of L_1, through perturbative calculations starting at the thin-torus limit. Details will be explored elsewhere.

Circumference and size dependence.—We illustrate the roles of N_s and L_1 by focusing on the four lowest levels of the $\mathcal{A}$-$\mathcal{A}$ tower, which form a diamond shape (e.g., Fig. 4). The ratio of the energy of the second $\Delta K_A = 0$ level to the first $\Delta K_A = 1$ level, each measured from the lowest $\Delta K_A = 0$ level, is an "aspect ratio" for the diamond shape, and is plotted in Fig. 3(b). Both the two-edge CFT picture and perturbation from the thin-torus limit predict aspect ratio = 2. This is seen to hold from the thin-torus limit up to some threshold value of L_1, which increases as N_s is increased. This situation is generically true for all CFT features: although the Laughlin state converges to CFT behavior at any L_1; at larger circumferences, more particles are required for finite-size convergence.

For large L_1 and finite N_s, the edges are close and therefore interact, leading to complicated effects such as the aspect ratio deviations seen in Fig. 3(b).
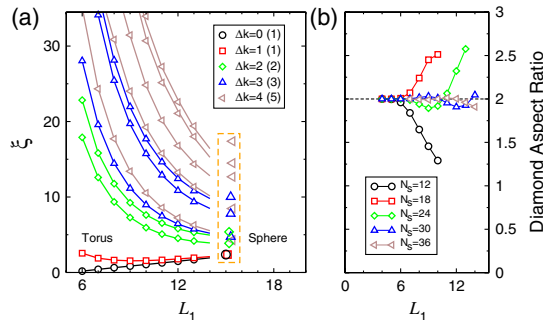

FIG. 3 (color online). (a) The chiral edge levels (type $\mathcal{A}$) identified from ES, as a function of torus thickness L_1. The rectangle contains the single-edge ES levels in spherical geometry [15], here scaled and shifted for best comparison with the torus results around $L_1 \sim 14$. (b) "Aspect ratio" of the diamond formed by the four lowest ES levels of the $\mathcal{A}$-$\mathcal{A}$ tower. The value 2 means a perfect diamond shape.
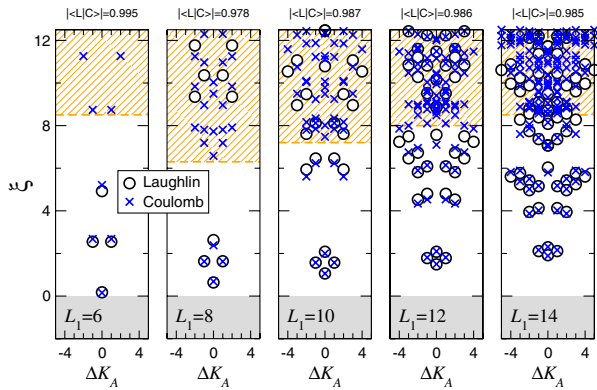
FIG. 4 (color online).   Comparison of the entanglement spectrum, and overlaps, between the Laughlin wave function and the Coulomb ground state for $L_1 = 6, \ldots, 14$ at fixed $N_s = 36$. Only the central part of the most prominent tower for the symmetric cut is displayed. We observe that the entanglement spectra of the two wave functions become very similar for sufficiently large L_1. The appearance of "generic levels" beyond the two-edge CFT picture in the Coulomb state is indicated by the shaded regions, leading to a tentative notion of "entanglement gap" [4].

Coulomb ground states.—The ES for ground states of the Coulomb Hamiltonian have more complicated L_1 dependence (Fig. 4). At smaller L_1, only the few lowest levels resemble the Laughlin ES; for $L_1 \lesssim 8$, the Coulomb ES cannot be generated using the two-edge procedure beyond the diamond structure. This does however not contradict the larger overlap between Laughlin and Coulomb states known at $L_1 \to 0$ [11,16] because the higher ES levels are pushed upwards at small L_1 (*cf* also Fig. 4). The ES thus exposes correlations much more subtle than is visible in overlap considerations. As L_1 is increased, more and more Coulomb ES levels match the Laughlin ES, and the emergent CFT tower structure can be seen.

Discussion.—This work presents entanglement spectra calculated through numerical diagonalization, for the Laughlin state at $\nu = 1/3$ on a torus. We presented two radically different physical ways of understanding the ES structure. The first interpretation is based on a combination of two chiral CFT edges. Each of these is individually similar to the edge spectrum previously extracted from ES studies on the sphere [15]. This interpretation is powerful as it reproduces the entire ES through the assignment of a few levels. Our second approach uses the adiabatic connection to the thin-torus limit, and the remarkable fact that the two-edge CFT structure is preserved even close to the thin-torus limit. Perturbative analysis based on the simple thin-torus states yields the locations and shapes of the towers, and many other quantitative predictions.

Accessing edge modes in explicit numerical calculations remains a highly desired but difficult task, due to edge reconstruction and other difficulties [7]. Our study of edge combinations through entanglement calculations provides an alternative track to gaining insight into this issue.

Our work opens up several important research directions, of which we list a few. We expect our results to have interesting generalizations to more intricate FQH states, such as the non-Abelian states.

Our data at large L_1 deviates from the independent-edges picture because the edges are close. The present setup thus provides the intriguing possibility of studying the interaction and interferences between two spatially separated edges, e.g., through exploring large L_1 features as in Fig. 3(b).

The CFT edge interpretation relies on the idea that the "entanglement Hamiltonian" is similar to the physical Hamiltonian. This notion is plausible but entirely unexplored for FQH states. There is thus a clear need for constructing and understanding entanglement Hamiltonians. It is also possible that a more detailed study of the CFT towers in the ES could yield Luttinger liquid features such as the compactification radius and more generally the scaling dimensions.

[1] L. Amico *et al.*, Rev. Mod. Phys. **80**, 517 (2008).
[2] A. Kitaev and J. Preskill, Phys. Rev. Lett. **96**, 110404 (2006).
[3] M. Levin and X. G. Wen, Phys. Rev. Lett. **96**, 110405 (2006).
[4] H. Li and F. D. M. Haldane, Phys. Rev. Lett. **101**, 010504 (2008).
[5] M. Freedman, M. Larsen, and Z. Wang, Commun. Math. Phys. **227**, 605 (2002); C. Nayak *et al.*, Rev. Mod. Phys. **80**, 1083 (2008).
[6] X. G. Wen, Phys. Rev. B **41**, 12838 (1990); **43**, 11025 (1991); **44**, 5708 (1991).
[7] X. Wan, K. Yang, and E. H. Rezayi, Phys. Rev. Lett. **88**, 056802 (2002); X. Wan, E. H. Rezayi, and K. Yang, Phys. Rev. B **68**, 125307 (2003); S. Jolad and J. K. Jain, Phys. Rev. Lett. **102**, 116801 (2009).
[8] N. Regnault, B. A. Bernevig, and F. D. M. Haldane, Phys. Rev. Lett. **103**, 016801 (2009).
[9] M.-C. Chung and I. Peschel, Phys. Rev. B **64**, 064412 (2001); I. Peschel and V. Eisler, J. Phys. A **42**, 504003 (2009).
[10] L. Fidkowski, arXiv:0909.2654v2.
[11] E. J. Bergholtz and A. Karlhede, Phys. Rev. Lett. **94**, 026802 (2005); J. Stat. Mech. (2006) L04001; Phys. Rev. B **77**, 155308 (2008); E. J. Bergholtz *et al.*, Phys. Rev. Lett. **99**, 256803 (2007).
[12] A. Seidel *et al.*, Phys. Rev. Lett. **95**, 266405 (2005).
[13] R. Tao and D. J. Thouless, Phys. Rev. B **28**, 1142 (1983).
[14] M. Haque, O. Zozulya, and K. Schoutens, Phys. Rev. Lett. **98**, 060401 (2007); O. S. Zozulya *et al.*, Phys. Rev. B **76**, 125310 (2007).
[15] O. S. Zozulya, M. Haque, and N. Regnault, Phys. Rev. B **79**, 045409 (2009).
[16] K. Yang, F. D. M. Haldane, and E. H. Rezayi, Phys. Rev. B **64**, 081301(R) (2001).